AN INTEGRATED SYSTEM OF
NUMERICAL SIMULATION AND VISUALIZATION
OF WAVE PENETRATION IN HARBORS

Eric C. Cruz
Associate Professor
Department of Civil Engineering
College of Engineering, University of the Philippines
Diliman, Quezon City, Philippines

ABSTRACT

An integrated system of numerical simulation and graphic visualization of penetration by waves in harbors has been developed for use in Windows-based personal computers. This paper discusses the wave transformation model behind the computational engine, its numerical implementation, the design and integration of a graphical rendering sub-system, and the application of the system to both theoretical and practical wave penetration problems. The system is capable of simulating in space and time the three-dimensional wave field based on a set of vertically-integrated, phase-resolving equations accounting for wave nonlinearity and frequency dispersion in the shallow water region around a harbor, as well as in the deep water region in the offshore area. The visualization component has been designed to provide quick and meaningful representation of both input and transient variables, with diagnostic capability for the rendering of input parameters and post-processing capability for the synthesis of wave field statistics. The system is validated by applying it to fundamental wave propagation problems where analytical or measured data are available for comparison. The computational and visualization capabilities of the system are demonstrated by its application to wave penetration studies of actual harbors.

I.   Introduction

Wave penetration refers to the propagation of incident waves from offshore into an enclosed area such as a harbor or bay. Penetration is possible through at least four mechanisms. The first is by wave propagation through the harbor's entranceway. The second is by wave energy transmission through interstices in the main body of protective structures such as porous breakwaters, jetties and quay walls. The third is by wave propagation over submerged structures such as natural or artificial reefs. And the fourth is by wave overtopping of fixed structures. In some cases, wave penetration may be due to a combination of these processes, as in submerged porous breakwaters where through-transmission and over-the-crest propagation are possible, or in low-crested solid structures where overtopping is significant, or in navigation entranceways protected by rubble-mound breakwaters where wave propagation, through-transmission and

overtopping may all be present. In this study, wave penetration by the first mechanism, namely, through gaps in fixed structures that vertically span the water depth, is considered. This mechanism of wave penetration is the most important in the propagation of wave energy into enclosed bodies of water. Structures in which the processes of through-transmission of wave energy, over-the-crest wave propagation and/or overtopping may occur are not considered.

The mechanism of wave penetration discussed above is governed primarily by the physical process of wave diffraction, and by the less dominant but equally important processes of wave refraction, wave breaking, wave reflection, bottom friction and nonlinear wave-wave interaction. In general, diffraction is induced by structures that obstruct the propagation of waves, regardless of the depth region where the waves propagate, whereas the less dominant processes occur as the waves reach the relatively shallow coastal area where the waves begin to "feel" the bottom. Wave diffraction, refraction and reflection can be treated mathematically by theories in wave mechanics (see Dean and Dalrymple, 1992), whereas wave breaking, bottom friction, and other physical phenomena observed in the nearshore zone, such as the generation of currents and existence of a mean wave set-up, can be described only with partial empiricism.

The propagation of sea waves over arbitrary bottom topography as affected by these physical processes is an important area of research in coastal engineering, and has been extensively studied and researched on over the last several years. A survey of wave models that have been proposed to determine the three-dimensional wave field is included in the next section. Although these models have varying degrees of reproducibility of the physical phenomena, as judged from their closeness to the analytical solutions and/or data measured either from laboratory experiments or from the field, their numerical implementation is an important issue that must be addressed if they are to be of wide practical use. Some of these models have been successfully coded into working computer programs. It is not the object of this study to discuss the mathematical bases of these models or their predictive capability as far as wave penetration is concerned. Rather this study aims to discuss the development of a system that integrates a numerical engine implementing one particular wave model for wave penetration analysis, and a suite of higher-level routines to graphically render the results into meaningful and easily visualized representation of the computed quantities. The output of this study is a modeling tool that can be run on personal computers by an engineer or researcher who may be engaged in various activities where wave penetration analysis is involved, such as engineering design, hydrodynamic analysis, construction planning and monitoring, wave hindcasting and forecasting, or purely scientific studies.

II.   Theory of Three-dimensional Wave Evolution

The process of evolution, or transformation, of waves from deep water in the offshore region to the shallow water near the shore has been significantly elucidated on in the last several years. This process is controlled by two important parameters, namely, the frequency dispersion and wave nonlinearity. Frequency dispersion, or dispersivity, determines the ability of the wave model to reproduce the relationship between the wave period and wavelength at arbitrary water depth h. Wave nonlinearity is a measure of the finiteness of the wave height relative to the water depth. If we denote the characteristic water depth by h, wave amplitude by a, and wavelength by l, then the dispersivity index is $\mu = h/l$ and the nonlinearity index is $\varepsilon = a/h$. In deep water, wave nonlinearity is insignificant and the transformation of waves is highly dependent on dispersivity. In shallow water, the wave amplitude increases due to shoaling while the wavelength decreases, leading to a rapid increase of wave nonlinearity. In intermediate depth, the transformation is equally dependent on both parameters.

In view of the possible wave conditions offshore and the wide range of water depths from offshore to the coast in wave penetration problems, it is important to use a wave evolution model that simultaneously treats the dispersive and nonlinear transformation of incident waves. Some of these wave models are discussed here. Berkhoff (1972) derived an evolution model called the mild-slope equation, which possesses the dispersion relation of linear wave theory. However, his model is limited to linear wave transformation and relatively mild slopes. Peregrine (1967) derived a set of vertically integrated equations, called Boussinesq equations, that treats nonlinear waves and has an inherent dispersivity that was limited to intermediate depths. By adding dispersion terms in the momentum equations, Madsen et al (1991) improved the dispersivity range of the Boussinesq equations up to the deep water region. Isobe (1994), using the concept of the Lagrangian and variational principle, derived a set of nonlinear, time-dependent governing equations for nonlinear random wave transformation. A nonlinear form of the mild-slope equation can be derived as a special case of the resulting model. By introducing functions for the vertical dependence of velocities and applying Galerkin method, Nadaoka et al (1994) developed a set of fully dispersive nonlinear wave model.
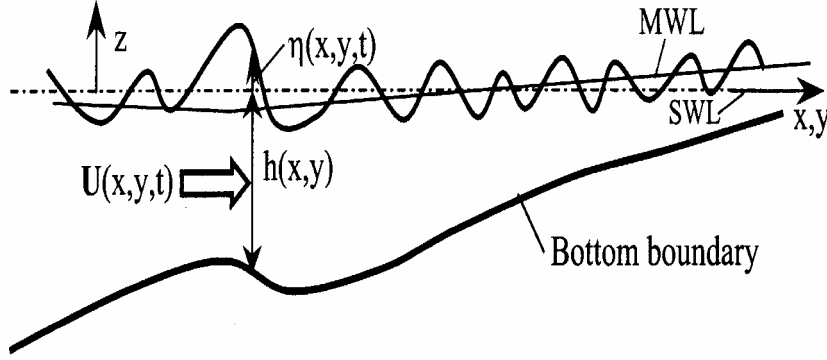
Fig.1 Definition of variables

In this study, the wave evolution model of Cruz et al (1997) is used to carry out the computations for wave penetration. This model is a subset of the general set of equations developed for arbitrary bottom topography that is overlain by an arbitrary permeable layer. The general model consists of the continuity equation and two sets of Boussinesq-type momentum equations, one each for the water layer and for the underlying impermeable layer. This was developed originally to study the wave fields around submerged porous breakwaters (Cruz, 1994; Cruz and Aono, 1998). In the current research, it is assumed that the sea bottom is fixed and impermeable, that is, the overlying layer is absent so that the variables for the fluid motion there can be dropped from the general equations. Hence for the horizontally two-dimensional wave transformation (**Fig.1**), the model equations used in this study are as follows:

$$\frac{\partial \eta}{\partial t} + \nabla \cdot \left[\mathbf{U}\left(h + \eta \right) \right] = 0 \tag{1}$$

$$\frac{\partial \mathbf{U}}{\partial t} + (\mathbf{U} \cdot \nabla)\mathbf{U} + g\nabla \eta + \frac{h^2}{6}\nabla\left(\nabla \cdot \frac{\partial \mathbf{U}}{\partial t} \right) - \left(\frac{1}{2} + \gamma \right)h\nabla\left(h\nabla \cdot \frac{\partial \mathbf{U}}{\partial t} \right)$$
$$- \gamma gh\nabla\left[\nabla \cdot (h\nabla \eta) \right] + \mathbf{F}_B + \mathbf{F}_S + \mathbf{F}_W + \varepsilon \mathbf{U} = 0 \tag{2}$$

Here $\eta(x, y, t)$ is the displacement of the free surface from mean water level, $\mathbf{U}(x, y, t)$ the horizontal velocity vector, $\nabla \equiv (\partial / \partial x, \partial / \partial y)$ the horizontal gradient operator, $h(x, y)$ the mean water depth, g the gravity acceleration, $\gamma = 1/15$ the dispersivity extension factor, x,y the horizontal coordinates, z the vertical coordinate, and t time. The velocity vector is defined as a depth-averaged value of the depth-varying horizontal velocity $\mathbf{u} \equiv (u, v)$:

4

$$\mathbf{U} \equiv (U, V) = \frac{1}{h + \eta} \int_{-h}^{\eta} \mathbf{u}(x, y, z, t) dz \tag{3}$$

Eq.(1), called the continuity equation, expresses the mass conservation law and is exact to all orders of ε and μ. Eq.(2), the momentum equation, is a vector equation which has a truncation error of $O(\varepsilon\mu^2, \mu^4, ...)$. Thus the model equations incorporate the leading order of wave nonlinearity, a property which is important in modeling wave evolution in shallow water. By using $\gamma = 1/15$ in the momentum equation, the dispersivity of the model is improved to have a reduced truncation error of $O(\mu^6)$, compared to that of the original model ($\gamma = 0$), which has an error of $O(\mu^4)$. This property is important in deep-water wave transformation, which is primarily governed by frequency dispersion. In wave penetration studies, the above orders of frequency dispersion and amplitude finiteness are deemed sufficient on account of the finite depth regime of the computation domain and the typical reduction of wave energy (proportional to the square of the wave height) inside the harbor due to partial enclosure by the structures. In addition, these model equations, when numerically implemented, will not require the use of too many grid points or higher-order derivatives that can render its discretization very cumbersome.

The coastal area around the harbor normally contains the surf zone, where waves break and undergo energy dissipation. Wave breaking is an extremely complex process that involves turbulence production, transport and decay, as well as sediment entrainment, suspension and transport. It is generally difficult to model wave breaking mathematically. However, it is possible to account for its effects by introducing an energy dissipation mechanism within the breaking zone. This is implemented by incorporating a wave breaking energy dissipation term $\mathbf{F}_B$ in the momentum equations. From previous studies, it has been found that the most appropriate dissipation term for spilling and surging breakers that are observed in many beaches is in the following form:

$$\mathbf{F}_B = -f_D \nabla^2 \mathbf{U} \tag{4}$$

Here f_D is a friction-type energy dissipation function whose form can be derived using linear wave theory but modified to account for finite-amplitude waves and other empirical characteristics of the breaking process. The breaking dissipation term is non-zero only within the breaking zone. In order to successfully account for the effects of wave breaking, it is important to locate the breaker line, or the zone where individual waves start to break. This is done by checking the maximum values of water elevations against the critical values from a specified breaking criterion. This criterion is typically semi-empirical and normally involves the relative depth h/l and the local bottom slope. The breaking dissipation function takes on a linear variation between the breaking point and the

5

point where the waves recover. The details of the wave breaking model are discussed in Cruz and Aono (1997a).

The term $\mathbf{F}_S$ is introduced into the momentum equation to account for energy damping by structures due to flow impedance, particularly near the corners. This is attributed to the existence of boundary layers that grow in thickness from the separation point along the fronting face of the structure. The resulting wake at the lee (relative to the flow direction) of the structure is a region of low momentum and will extract energy from the main body of the flow. Thus, the structure damping term is expressed in terms of a momentum exchange mechanism, as follows:

$$\mathbf{F}_S = -\nabla \cdot (\sigma \nabla \mathbf{U}) \tag{5}$$

Here σ is a flow-dependent semi-empirical momentum-exchange coefficient that is proportional to the transient total depth, as follows:

$$\sigma = \alpha_m \sqrt{g} (h + \eta)^{3/2} \tag{6}$$

The nondimensional coefficient α_m varies between zero and unity, takes on a maximum value at a structure discontinuity, and rapidly decays to zero within a short distance. The negative sign in Eq.(5) accounts for the change in direction of momentum transport as the velocity reverses as a result of the oscillatory flow of wave motion.

In the shallow coastal area, the penetration of horizontal velocities throughout the entire depth induces a friction resistance at the bottom, which acts to impede wave motion. Although the exact nature of bottom friction depends on the characteristics of the bottom boundary layer in shallow water, the bottom friction resistance $\mathbf{F}_W$ is modeled as a nonlinear term in the horizontal velocities and inversely proportional to the total water depth, with a uniform nondimensional friction coefficient f_w, as follows:

$$\mathbf{F}_W = \frac{f_W |\mathbf{U}|}{2(h + \eta)} \mathbf{U} \tag{7}$$

The absolute value in Eq.(7) makes certain that bottom friction always acts opposite the direction of velocity. The fact that bottom friction is small in deep water and significant in the shallow coastal area is correctly reflected by Eq.(7).

III. Boundary Conditions

A. Open boundaries

Computations are carried out in a finite rectangular area. The location of the offshore boundary is determined such that the effects of scattered waves from the interior are negligible and that bottom sediment movement is nil. The location of the lateral boundaries is chosen such that they act as open boundaries, where outgoing waves are allowed to propagate out of the domain without artificially generating reflected waves that may muddle the results in the interior. The remaining boundary is usually a physical boundary such as a wall, where wave reflection and dissipation can occur, or a beach where the shoreline is mobile and the transient total depth is zero.

The lateral boundaries should be as distant from the area of interest as possible to minimize the possible re-reflection of outgoing scattered waves. However, this would require large computer storage and computing time because of the resulting large number of grid points and the long time for the propagating waves to reach these boundaries. In practical computations, the location is chosen such that the resulting region is computationally manageable and that the resulting direction of the propagating waves in the interior as affected by bottom topography is almost parallel to the lateral boundaries, so that anticipated artificially generated reflected waves are negligible. In many cases, however, the bathymetry of the area and the character of the incident waves may make this procedure difficult to apply.

In this study, the open boundary condition is enforced by attaching an auxiliary region or layer at the fictitious lateral boundary. This so-called "sponge layer" or "numerical wave absorber" effectively absorbs the outgoing scattered waves. The sponge layer is characterized by a constant width F and a prescribed boundary damping distribution ε. For example, for a sponge layer parallel to the x-axis, the damping distribution is given by

$$\varepsilon = \varepsilon(y) = \varepsilon_m \sqrt{\frac{g}{h}} \frac{N+1}{2F^N}(y - y_F)^N \tag{8}$$

where y_F is the location of the lateral boundary, N the order of distribution (N = 1 if linear, N = 2 if parabolic), and ε_m a nondimensional maximum damping coefficient. At the lee side ($y = y_F + F$) of the absorber, the Sommerfeld radiation conditions are applied, namely:

$$\frac{\partial \eta}{\partial t} + C \frac{\partial \eta}{\partial y} = 0 \tag{9}$$

$$\frac{\partial U}{\partial t} + C\frac{\partial U}{\partial y} = 0 \tag{10}$$

The wave celerity C is taken as the frequency-independent celerity $\sqrt{gh}$, where h is the depth at the boundary. The derivatives in Eqs.(9) and (10) are evaluated at the lee of the sponge layer. The absorber width is fixed before the simulation, typically at 10h, and the resulting number of additional grid points in the auxiliary layer is verified to be manageable. The properties N and ε_m of the sponge layer, are determined from the simulation aid graphs theoretically developed by Cruz and Isobe (1994) such that for a maximum reflection of 3% and selected damping width, the range of absorbable frequencies covers relative depths of 0.040 to 0.50. In general, the parabolic absorber is more efficient, that it utilizes a smaller width, in absorbing short waves. It is also more effective in absorbing dispersive wave packets normally associated with irregular waves.

B. Structure boundaries

The interaction of waves with fixed structures is implemented through an internal boundary condition. This considers the spatial variability of the structure's material make-up and face slope, which results in varying reflectivities along its length. This boundary condition also treats incoming waves with a wide range of frequencies and incoming directions. A suitable boundary condition that can handle these actual field conditions has been obtained based on the resolution of volume flux (Cruz and Aono, 1997b). This condition is also compatible with the discretization of the wave model based on finite differences. For a structure oriented arbitrarily relative to the incoming wave direction or coordinate axes, the boundary condition applied to the x-direction relates the properties of the reflected wave with those of the incoming wave taken at different times, as follows:

$$\left[U(h+\eta) \right]^t \Big|_{(x,y)} = |F_{xx}| \left[U(h+\eta) \right]^{t-\tau_x} \Big|_{(x\pm\Delta x,y)} \tag{11}$$

$$F_{xx} = \frac{\cos\alpha_i + r\cos\alpha_r}{\left\{ \left\{ \cos^2\alpha_i + r^2\cos^2\alpha_r + 2r\cos\alpha_i\cos\alpha_r\cos\left[k\Delta x \left(\cos\alpha_i - \cos\alpha_r \right) \right] \right\} \right\}^{1/2}} \tag{12}$$

Here, x, y are the coordinates of the boundary, Δx the grid spacing, t time, r the reflection coefficient at the current grid, α_i the incident wave direction, α_r the reflected wave direction, and $k\,(=2\pi/L, L\text{: wavelength})$ the incoming wave number. The reflection coefficient can vary along the structure length, The time

lag τ_x is obtained from its value normalized by the incoming wave frequency $\omega(= 2\pi/T, T : \text{wave period})$ from the equation below:

$$\tan \varpi \tau_x = \left| \frac{\cos \alpha_i \sin(k\Delta x \cos \alpha_i) + r \cos \alpha_r \sin(k\Delta x \cos \alpha_r)}{\cos \alpha_i \cos(k\Delta x \cos \alpha_i) + r \cos \alpha_r \cos(k\Delta x \cos \alpha_r)} \right| \tag{13}$$

The wave number is obtained from the wavelength of the wave component impinging on the boundary. The wave frequency is related to the water depth and wave number through the dispersion relation of the wave model, namely:

$$\omega^2 = \frac{gk^2(1 + \gamma k^2 h^2)}{1 + (1/3 + \gamma)k^2 h^2} \tag{14}$$

The directions of the incident and reflected waves are related through the orientation angle β of the structure reckoned from the x-axis, as follows:

$$\alpha_r = 2\beta - \alpha_i \tag{15}$$

For regular waves, the incident wave direction can be determined from the magnitudes of the horizontal velocities U and V. For irregular waves, a method based on time averaging of the wave field variables is discussed in Cruz and Aono (1997b). A parallel development is done for the y-direction, leading to analogous equations involving the velocity V.

IV. Numerical Simulation of Wave Penetration

Model Discretization

The finite difference method is used to discretize the mathematical model, in view of the time-marching requirement for the solution and of the structure of the boundary conditions. In wave penetration analyses, the marching period must be estimated such that the simulated time series capture a significant number of individual waves for use in wave statistical analysis. On account of multi-reflection within the harbor, the prevailing wave field is normally established after a long simulation period.

For a given bottom topography, structure alignment, reflection coefficients, and incident wave conditions, the solution computes η and the velocities U,V at all grid points for all times. Each of these variables is defined on spatial grids, which are mutually staggered in space, such that the η values are defined on the grid intersections, and the U and V values are between the intersections along the x- and y-directions, respectively. The velocity grids are spaced by a time step of Δt but staggered relative to each other, while the η grids are marched in time with a finer step of $\Delta t/2$. The wave model and boundary

9

conditions are reduced to algebraic equations using an alternating-direction-implicit (ADI) scheme that solves η, U and η, V in alternate fashion. Each time-marching step uses two sweeps, each involving an implicit scheme for the component momentum equation to obtain the velocities in that coordinate direction, and an explicit scheme for the continuity equation to obtain η. The boundary conditions for the sponge layer and structure boundaries are discretized using a compatible approach. The discretization and numerical solution methods are similar to those discussed in Cruz et al (1997b).

Numerical Simulation Parameters

Numerical simulation commences from still water conditions. It is important to introduce the incident wave into the computation domain quite slowly in order to avoid singularities due to the nonlinearity of the wave model. This is done by multiplying the time series of incident water elevations by a linear variation with time from zero to unity, over a fixed lead time, typically equal to two incident wave periods. It is also important to employ an appropriate wave generation method to introduce the incident wave train without interfering with the outgoing scattered waves. An interior wave generation technique similar to that used by Ishii et al (1994) for linear random waves was applied in this study.

The selection of grid size and time step is critical because of the long simulation time required to obtain the wave field. The grid size and time step are fixed at the start of simulation between $L/20$ to $L/10$ and $T/20$, L and T being the incident wavelength and period. This range of grid size is also sufficient to discretize the structures. For irregular waves, the applicable wavelength and period are based on the incident significant wave. The chosen grid size and time step are considered small enough to resolve the high frequency components of the transformed waves throughout the range of known water depths, yet coarse enough to obtain the results in a reasonable amount of time. Simulation is terminated when at least 20 constant-amplitude waves have been obtained at the shore boundary for regular waves, and at least 2048 individual waves have been obtained at the shore boundary for irregular waves. These numbers are sufficient to synthesize the wave heights and other statistics from the resulting time series using the method of individual wave analysis (Goda, 1985).

Computation Domain for Wave Penetration in Harbors

Wave penetration analyses are typically carried out to determine the level of agitation of the water surface inside an enclosed structure induced by waves that enter through a fixed opening, such as a navigation entranceway or the mouth of a bay. In this case, the computation domain is selected to include only the structure and the opening, and the incident wave conditions are introduced at the opening (Sato et al, 1990). The treatment of outgoing scattered waves leaving the opening is implemented through an open boundary condition. This approach, however, precludes the interaction of the structure's interior with the exterior, and

thus neglects the coupling of these wave fields through the opening. While this may be reasonable in certain situations, the approach is very limited in many cases. One such case is when wave breaking occurs in the exterior, which significantly alters the wave field due to the currents induced by breaking. These currents can penetrate the interior through the opening. Another is when there is appreciable reflection from the exterior faces of the enclosing structure, such as breakwaters, so that the reflected wave energy can propagate into the interior.

To properly account for the coupled hydrodynamics in the interior and exterior, the approach recommended here is to select a computation domain that is reasonably vast to contain the immediate exterior region and to select the location of incident wave generation in sufficiently deep water. In this manner, the opening implicitly becomes an alignment of interior grid points and hence need not be treated in a special way. At the same time, the scattered outgoing waves can leave freely, while the propagating waves in the exterior can penetrate the harbor freely. Since the structure faces are internal boundaries, only the structure boundary condition needs to be enforced there. With this approach, it is possible to study not only the level of agitation inside the harbor but also the wave field outside of it. Such information is very important when assessing, for example, the suitability of the harbor for navigation, which is highly dependent on offshore tranquility.

The recommended approach above may have disadvantages. The first is, of course, the increase in memory requirement and computation time as a result of the resulting larger computation domain. The other is the necessity for a separate treatment of the shore in the exterior, where a moving shoreline may exist. This will require a special boundary treatment and further extend the computation domain since additional grid points must be introduced to contain the moving boundary. The practical alternative suggested here is to terminate the shore boundary at a very shallow depth and attach the sponge layer there, thereby allowing reflection to occur without the need to introduce additional grid points or to enforce special conditions.

V.   Graphic Visualization Suite

Graphical rendering of the wave field variables and other data was made possible by invoking a set of application programs based on the PGPLOT graphics subroutine library. This library is a Fortran- or C-callable, device-independent graphics package for making simple scientific graphs of publication quality with minimum effort on the part of the user. Most application programs based on this library can be device-independent, and the output can be directed to the appropriate device at run time. The PGPLOT library consists a device-independent part and a set of device-dependent "device handler" subroutines for output on various terminals, image displays, dot-matrix printers, and pen plotters. Common file formats include PostScript and GIF.

PGPLOT itself is written mostly in standard Fortran-77, with a few non-standard, system-dependent subroutines. PGPLOT subroutines can be called directly from a Fortran-77 or Fortran-90 program, but a binding library is provided that allows the library to be called from a C or C++ program. PGPLOT consists of open-source codes that are freely available for non-commercial users, and has been tested on UNIX and OpenVMS operating systems. The source code and documentation are copyrighted by the California Institute of Technology, where it was developed for use in astronomical data reduction programs (http://www.astro.caltech.edu/~tjp/pgplot/).

The application libraries, called APPLI2D and APPLIXY, consist of subroutines for rendering two-dimensional plots and plots of x-y data pairs, respectively. APPLI2D includes routines for plotting color maps (see **Fig.9**, **10** for examples), marking routines (see **Fig.11** for example), contouring routines (see **Fig.13** for example), and combination routines (see **Fig.6** for example), among others. APPLIXY consists of routines for plotting lines and curves and marking data. Both libraries are capable of overlaying plots, which is useful for superimposing structures and other boundaries, and in studying the temporal changes of variables of interest. They are capable of directing the output to the display, which is useful for diagnostic purposes, or to a file of a specified format for subsequent printing. Initially, the format for file output is Postcript, but can be easily extended to other formats through the proper device handler subroutine of PGPLOT.

The design of the user interface for the visualization suite is a time-consuming task. With a view to quickly call APPLI2D and APPLIXY without the necessity of developing graphical interfaces, parameter files that set the graphic parameters to control the outputs of the application libraries are chosen to provide the user-interface. These parameter files are designed as text files that contain textual descriptions and placeholders for interactive graphic control and ease of editing with a text editor. They are created within the simulation program at different stages of the run, and can be used for code debugging, input data diagnostic, pre-simulation diagnostic, post-simulation processing, and simple animation. The options for graphic control are designed as wide as possible so that the application libraries can be easily integrated into other numerical simulation systems. In the current integrated system, the parameter files are suited for wave penetration analyses. The development of the graphic visualization component is discussed in more detail in a separate paper (Cruz, 2003).

VI. Validation of the System

A. Diffraction around a semi-infinite breakwater

Diffraction is the dominant process in the wave penetration of enclosed structures. Accordingly, the capability of the wave model is validated first against this process by testing it for the diffraction of small-amplitude waves around a

semi-infinite breakwater in water of uniform depth. The breakwater is assumed to be very thin with fully reflective faces. For the general case of oblique wave incidence, an analytical solution was obtained by Penney and Price (1952) in terms of Fresnel integrals, but its numerical computations involve complex numbers. For normal wave incidence, an analytical solution, which is computationally simpler, is available in Dean and Dalrymple (1992). This solution yields the diffraction coefficient, or ratio of local wave height to incident wave height, at any location around the breakwater.

In the numerical simulation, the incident wave conditions were specified to have very small wave nonlinearity ($H/h = 0.10$) to be consistent with the assumptions of linear wave theory. An intermediate water depth ($h/L_0 = 0.23$, L_0 is the deepwater wavelength) was also chosen to simultaneously test the dispersion property. The simulation was carried out with regular incident waves and was terminated when running values of wave heights at the shore boundary had become practically constant. Since the breakwater needs to be thin, a fine grid spacing of $L/20$ was set. **Fig.2** shows a simulated transient three-dimensional wave field for a wave incident from the upper left. The propagation zone of virtually constant wave height, shadow zone of diffracting waves, and the fronting reflection zone of standing waves are all visible. The auxiliary zone for wave absorption is also visible, and the magnitude of the outgoing reflected wave from the fronting face can be gleaned in the offshore absorption region.

The comparison of diffraction coefficients at various sections is shown in **Fig.3**. Along a transverse section in front of the structure (y = -L), the propagation zone has the expected constant diffraction coefficient, and in the reflection zone (y = L) values that oscillate about 2.0. The small values in the shadow zone are prominent in the longitudinal sections, and along the geometric line (x = 0) between the propagation and shadow zones, the coefficient approaches an asymptote of 0.50, which is a known typical behavior of diffraction patterns for semi-infinite breakwaters. Two runs of simulation were executed; in the linear wave simulation, the nonlinear terms in the wave model were switched off. It is clear that the simulated wave heights agree well with theory. Wave nonlinearity is relatively inconsequential, except at the high points where the peaks are somewhat magnified. The dispersion property is also very accurate since the locations of the resulting minima and maxima coincide in the theory and simulations.
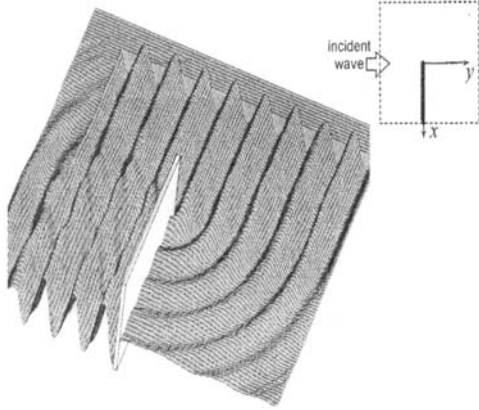
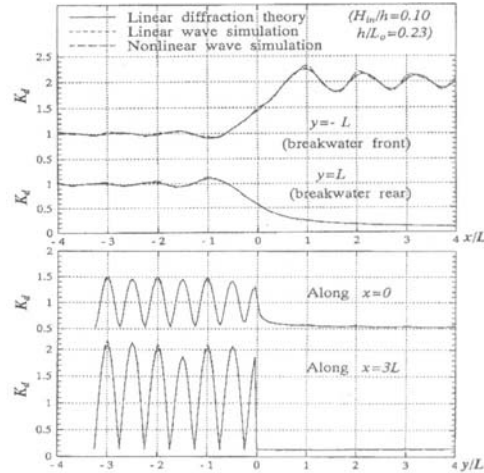**Fig. 2** Simulated diffraction around a semi-infinite breakwater

Fig. 3 Comparison of diffraction co-efficients for semi-infinite breakwater

B. Diffraction around a rectangular island

Diffraction of waves by a rectangular island was simulated using this system. Unlike the semi-infinite breakwater, an island has finite lengths and comparable dimensions in orthogonal directions, which imply that wave penetration takes place around both edges, and that energy dissipation may exist due to the momentum exchange at the lee near the corners. When the island dimensions are small relative to the incident wavelength, the structure may degenerate into a point structure, so that diffraction effects are negligible. Accordingly, the dimensions were chosen large enough for wave penetration into the shadow zone to be significant.

Fig.4 shows an instantaneous water surface configuration simulated by this system, depicting the evolution of initially long-crested incident waves into short-crested waves in all directions. The scattered waves that return offshore are also prominent. **Fig.5** shows the resulting distribution of diffraction coefficients along a transverse section several wavelengths behind the island, together with measured wave heights on a physical model for the island. The wave heights are clearly reduced at the central lee section while those within the propagation zone are generally magnified as a result of superposition of wave components from both sides. Two nonlinear simulations were carried out, in which the structure-damping coefficient α_M of eq.(6) was set to zero and 0.5 in separate runs. The effects of this damping mechanism are highest along the oblique lines at the back commencing from the down-wave corners, where the component waves add up to amplify the wave height. As seen from the results, the existence of this damping mechanism improves the agreement with measurements for the larger wave heights.
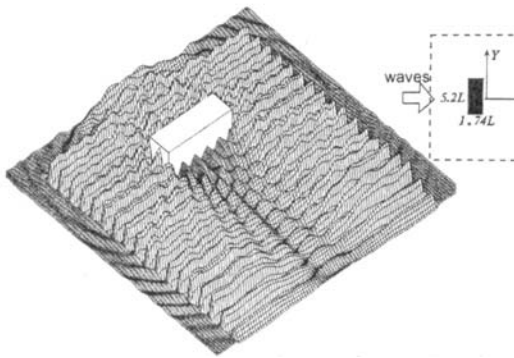
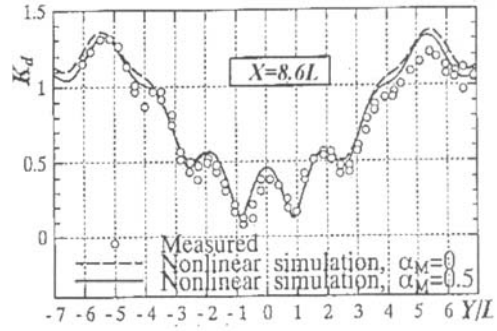**Fig. 4** Simulated wave field around a
rectangular island

Fig. 5 Comparison of wave heights
behind a rectangular island

C. Simulation of penetration by sea waves into a prototype harbor

The integrated system has been applied in the study of the wave field around an existing harbor. This prototype structure is formed by sloping-face concrete breakwaters, has a single opening, and encloses a basin area of approximately 6.3 hectares (**Fig.6**). It has two bays that are separated by relatively shorter breakwaters with two entranceways. The mean depth in the interior basin is about 2 to 3 meters. The harbor is located along a coastline and near a river mouth, which is known to discharge significant sediments into the adjoining sea. **Fig.6** shows the bottom configuration around the harbor at the time of field measurements. In the application of the above system, the properties of the significant wave synthesized from a continuous two-month measurement of the water surface elevations and water particle velocities were used for comparison. The field measurements involved 6 gauging stations as shown in **Fig.6**. Station 1 is mounted at a depth of about 21 meters in the offshore region, where the effects of the waves scattered by the harbor and the seabed are assumed to be negligible. Station 2 is in front of the harbor entrance, Station 3 is in the outer bay and 3 stations are sited in the inner bay.
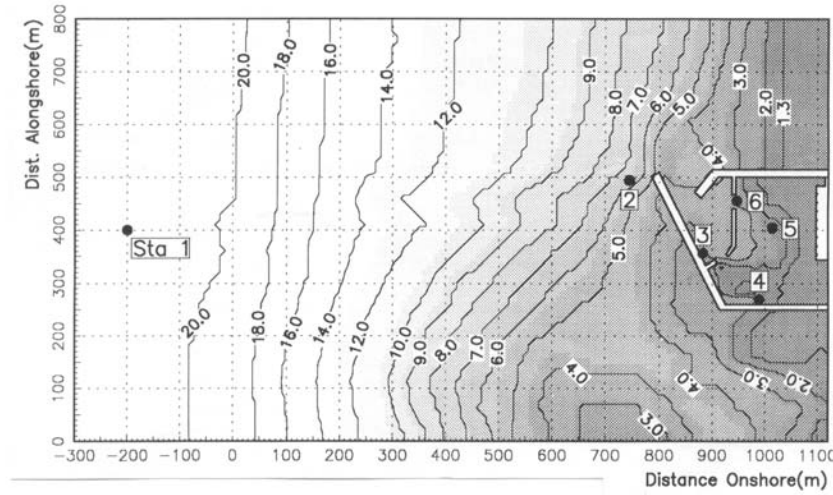
15

Fig.6 Bathymetry around a prototype harbor, and location of gauging stations

The bathymetric region (shown as the innermost dashed rectangle in **Fig.9)** measures 800 meters by 1000 meters, and with domain extensions for the boundary-damping region and interior wave generation, the computation domain covers an area of 1050 meters by 2000 meters. Field data for normal wave incidence, where the waves approach the shore at right angles, were used for comparison. The measured water elevations at all stations indicate the presence of so-called infra-gravity waves, which possess periods of 1 minute and higher, together with the usual sea waves, with periods of about 5 to 15 seconds. For the interior wave generation, the measured random water surface displacements at Station 1 were synthesized using frequency analysis, and the significant wave heights and periods were obtained. The resulting frequency and amplitude spectra, as shown in **Fig.7** including the low-frequency infra-gravity waves, are then converted to time series of water elevations and particle velocities, as shown in **Fig.8**, using linear wave theory with random phase differences. These time series serve as the boundary conditions at the wave generation line.
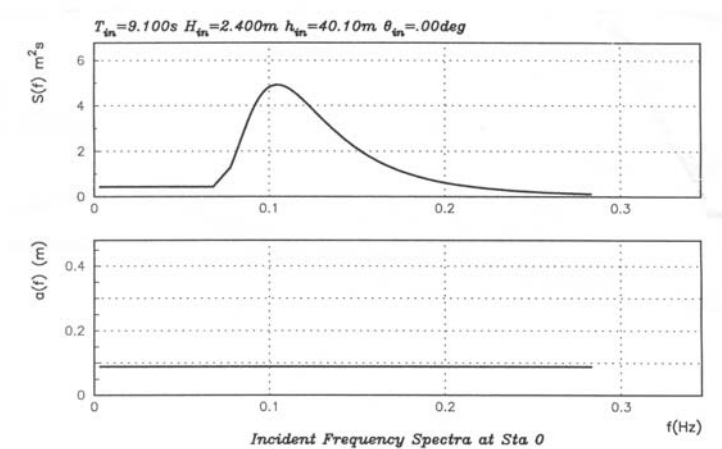

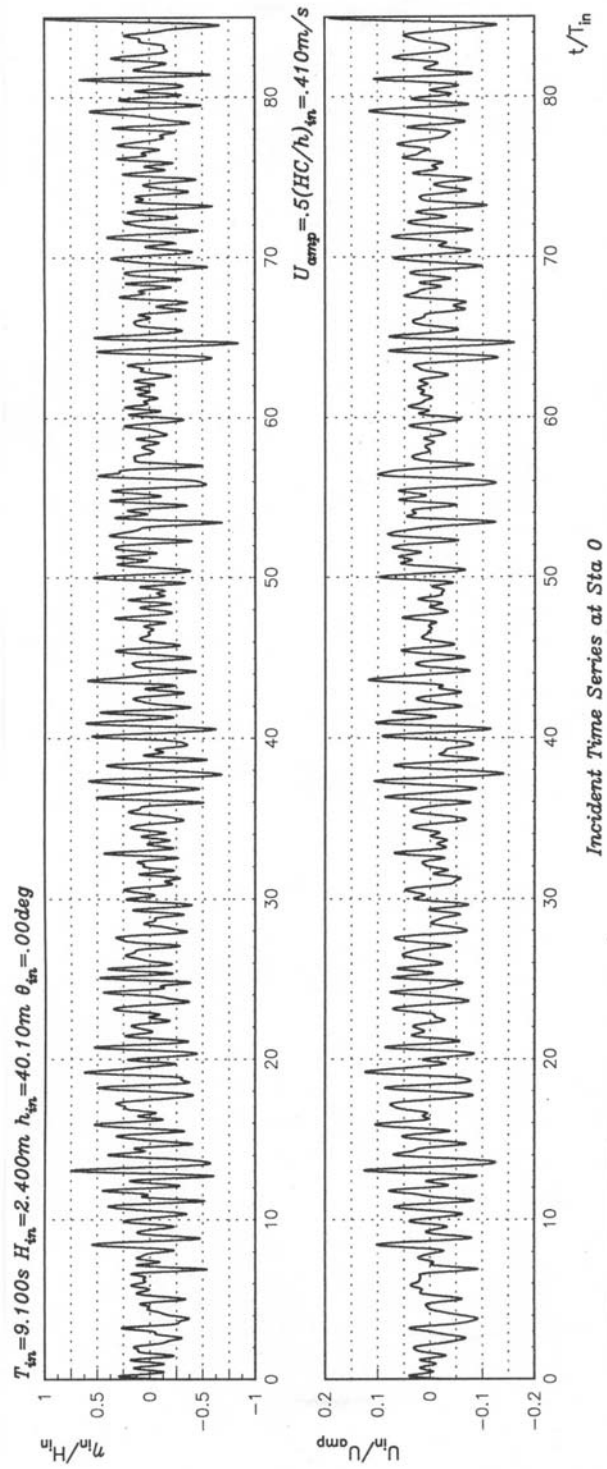**Fig.7** Frequency and amplitude spectra of incident wave at Station 1

Fig.8 Prescribed water elevations and horizontal velocities of incident wave

17

Figs.9 and 10 show spatial distributions of the water surface displacements $\eta(x,y)$ at two time instances for one simulation run, where the generation and propagation of the scattered waves from the harbor, as well as the penetration of the incident waves into the harbor, can be visualized. Inside the open boundary divide, the resultant η is shown, and outside this divide, η of only the outgoing scattered waves is plotted. The images also show the action of the boundary damping regions, which dissipate the outgoing waves as they leave the domain. **Fig.11** shows the transient breaker segments, where wave breaking is detected according to the breaking criterion, while **Fig.12** shows the corresponding spatial distribution of the energy dissipation function f_D in eq.(4) for this instance. It is seen that breaking occurs near the coast, where the water depth is shallow, and in front of the oblique breakwater, where the interaction of the reflected and incident waves cause a steepening of the wave profile. In general, wave breaking is not observed inside the harbor.
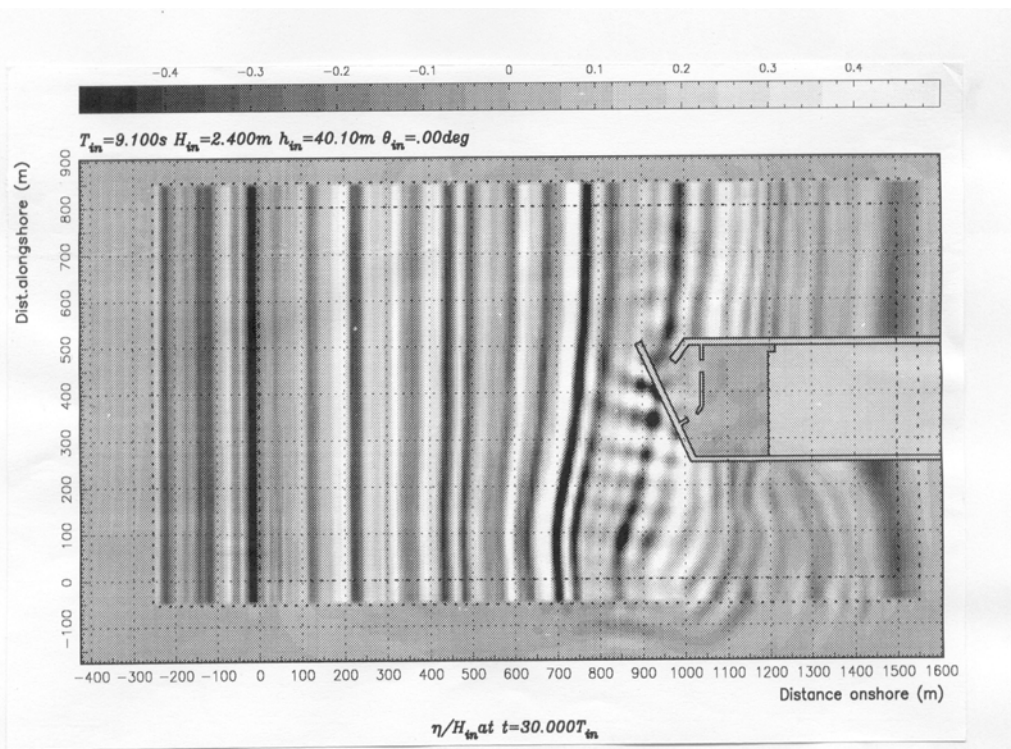

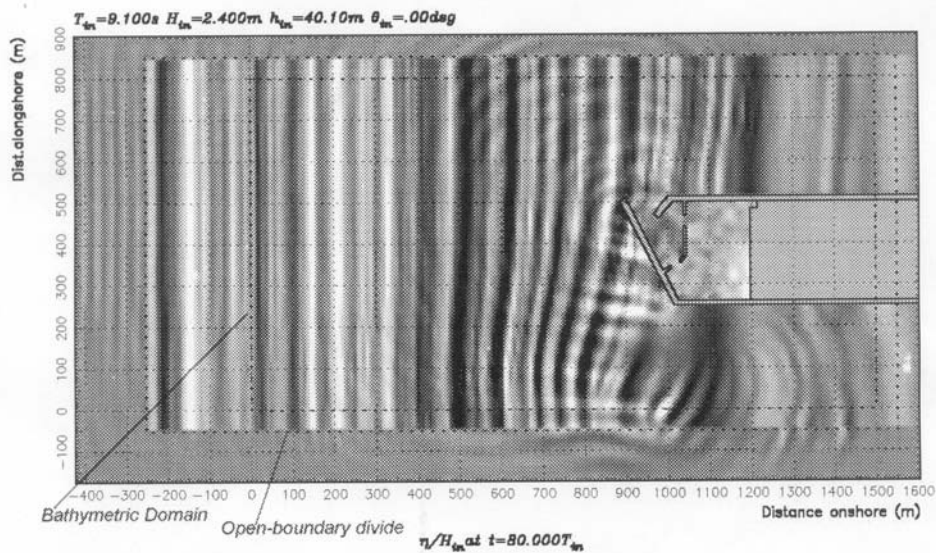**Fig.9** Simulated transient (normalized) wave field

$T_{in}=9.100s$ $H_{in}=2.400m$ $h_{in}=40.10m$ $\theta_{in}=.00deg$

Dist.alongshore (m)

Bathymetric Domain   Open-boundary divide

Distance onshore (m)

η/H_{in} at $t=80.000T_{in}$

Fig.10 Simulated (normalized) wave fields at a later instance.

Figs.9 to **12** demonstrate that wave penetration is influenced by the wave field outside the harbor, and a simulation that decouples the interior and exterior hydrodynamics will be erroneous. However, it is valid to deduce that such coupling may be relaxed when the harbor entrance is very small relative to the basin area so that the interaction is limited to a small region around the entrance.

$T_{in}=9.100s$ $H_{in}=2.400m$ $h_{in}=40.10m$ $\theta_{in}=.00deg$

Dist.alongshore (m)

Distance onshore (m)

Breaker Segments at $t=30.000T_{in}$
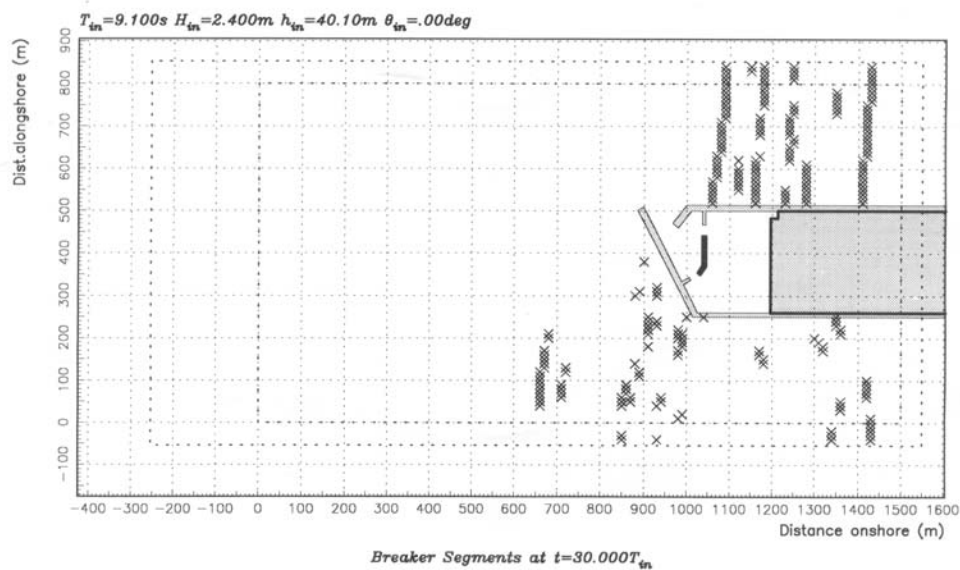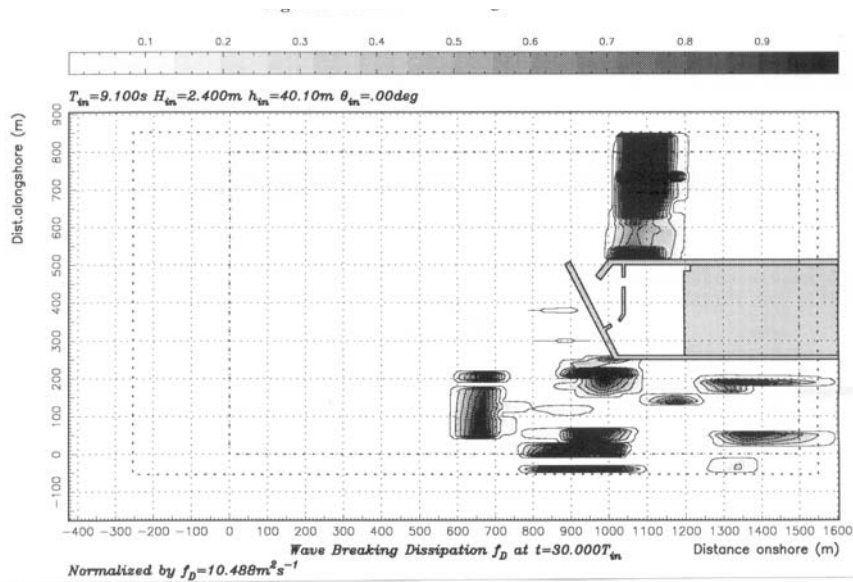
Fig.11 Simulated breaker segments

19

Fig.12 Simulated (normalized) breaker zones

Fig.13 shows the spatial distribution of the significant wave height inside the harbor, which was synthesized after about 1024 waves have been recorded at the Station 5. **Fig.14** shows the spatial distribution of the corresponding significant wave period. It is seen that the wave heights inside the harbor are reduced significantly due to wave blocking by the breakwaters. While there are localized concentrations of wave energy near the partially reflective walls in both outer and inner bays, there is a diffusion of energy in the inner bay due to its larger basin area. **Fig.14** shows that the significant period is generally reduced by about 5 to 15 percent in the harbor interior. Such information is important when the harbor is to be used for fishery, since the loading/unloading of fish catch is often dependent on the ambient wave period near the docks.
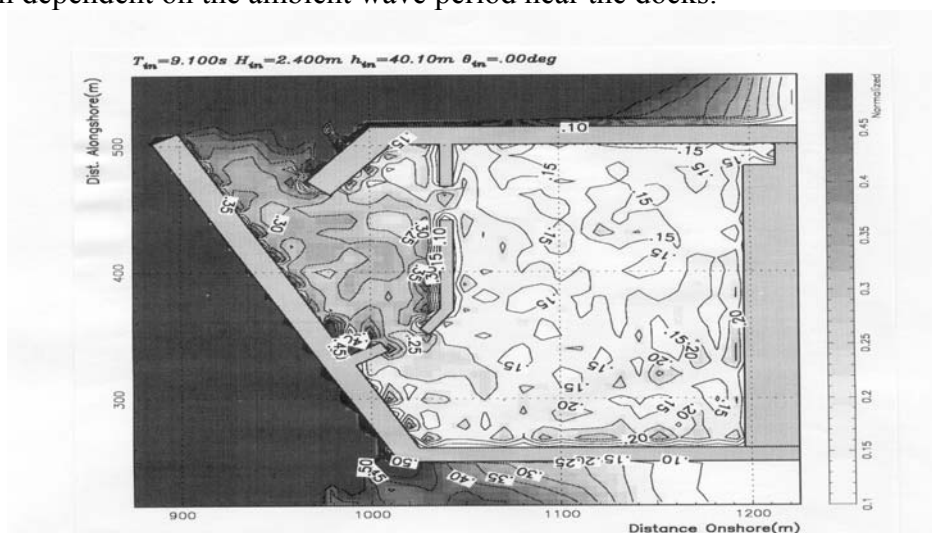

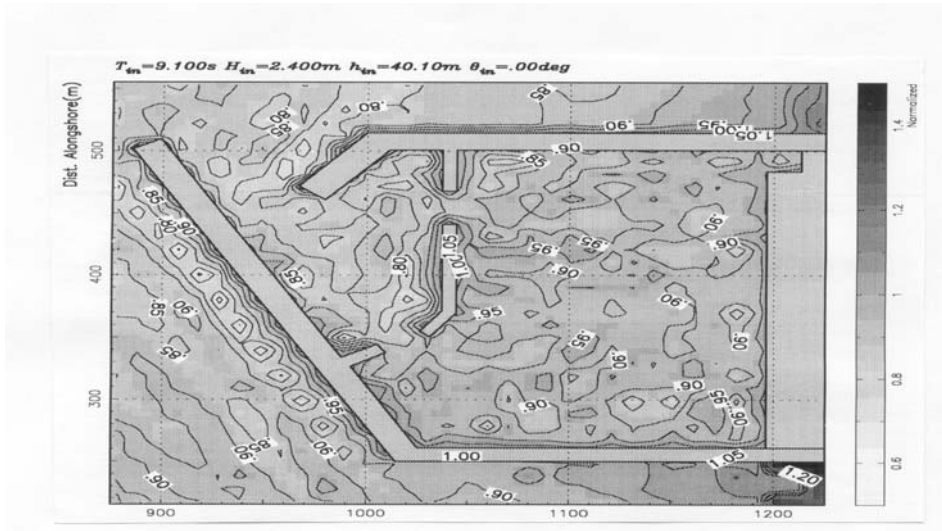**Fig.13** Spatial distribution of (normalized) significant wave height

20

Fig.14 Spatial distribution of (normalized) significant wave period

Fig.15 shows the comparison of the significant wave heights at Stations 1, 2, 4 and 5 for three cases of incident sea waves, which are summarized in Table 1. **Fig.16** shows the comparison of the corresponding significant periods. It is seen that, notwithstanding the differences in the conditions of the field measurements and the numerical simulations, the present system correctly predicts the variation of the wave heights and periods. The height of the sea waves is significantly reduced as the incident waves penetrate the harbor, partly due to the transfer of wave energy from the high-frequency sea waves to the low-frequency infragravity waves by nonlinear wave-wave interactions, and partly due to wave transformations outside the harbor due to refraction, wave breaking, and damping. There is a slight over-estimation of the wave heights at Stations 2 and 5 by the model, which may be due to the previously mentioned differences in the measurement and simulation conditions. The evolution of the significant wave period is more gradual. As seen in **Fig.16**, wave penetration results in a decrease of the wave period inside the harbor. The last two figures also indicate that the wave height inside the harbor is only weakly dependent on its value in the offshore region, whereas the period inside the harbor is proportional to its value in the offshore region.

Table 1
Cases of Incident Wave Conditions

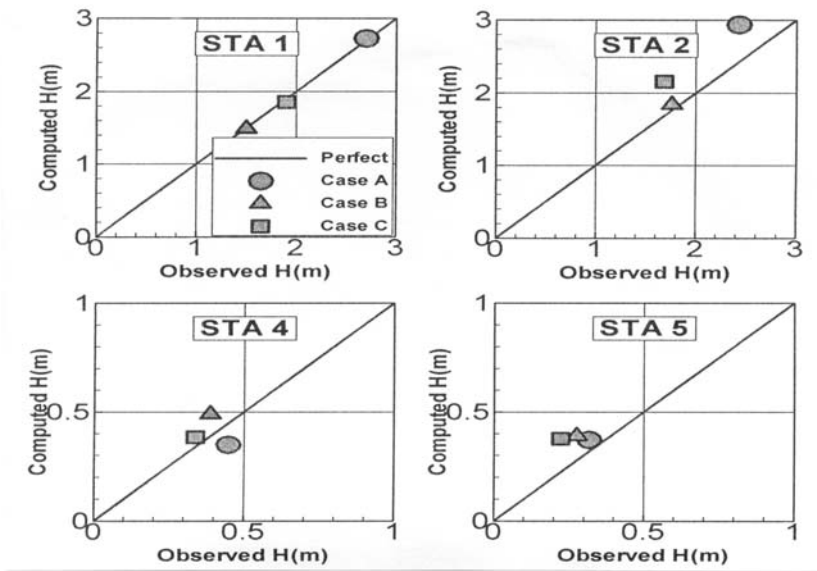| Case	Incident Significant Wave		Remark
	Period	Height	
A	Nominal	Nominal	Nominal sea wave
B	Long	Low	Long sea wave
C	Nominal	High	High sea wave

21

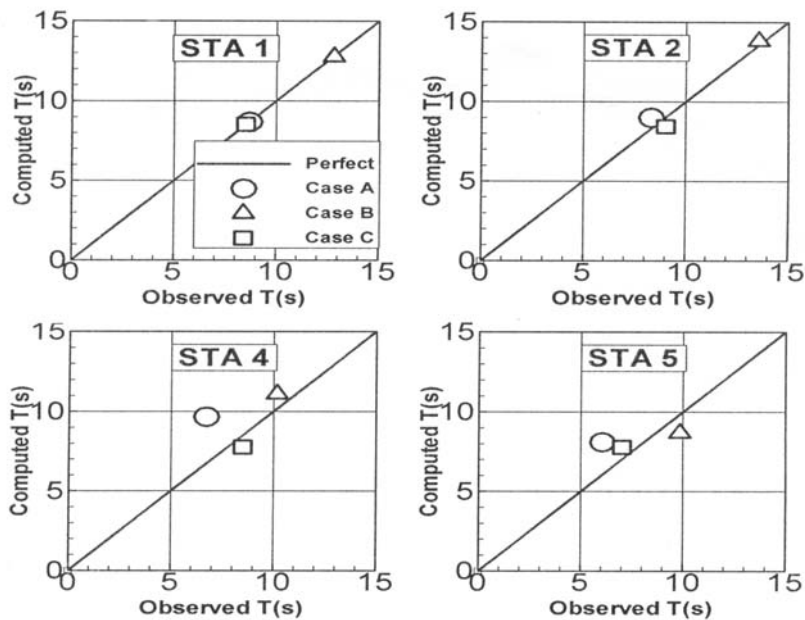**Fig.15** Comparison of significant wave heights of sea waves

Fig.16 Comparison of significant wave periods of sea waves

VII.   Application of the System to Studies of Wave Penetration in Harbors

The integrated system above was applied to studies of actual harbors for various purposes. In one application for a harbor being built to serve as a trans-shipment hub, the system was used to determine the wave climate around the open spaces temporarily created by the construction of segments of breakwaters (**Fig.17**). The information on the ambient and maximum wave heights was to be used by design engineers to evaluate the structural adequacy of the breakwaters. A more important objective is the provision of graphic images of the wave fields to field engineers for the purpose of monitoring construction. As shown in **Fig.17**, an integrated system of analysis and visualization is very useful in providing quick, accurate and concrete images of the wave climate under arbitrary transient conditions of the site.
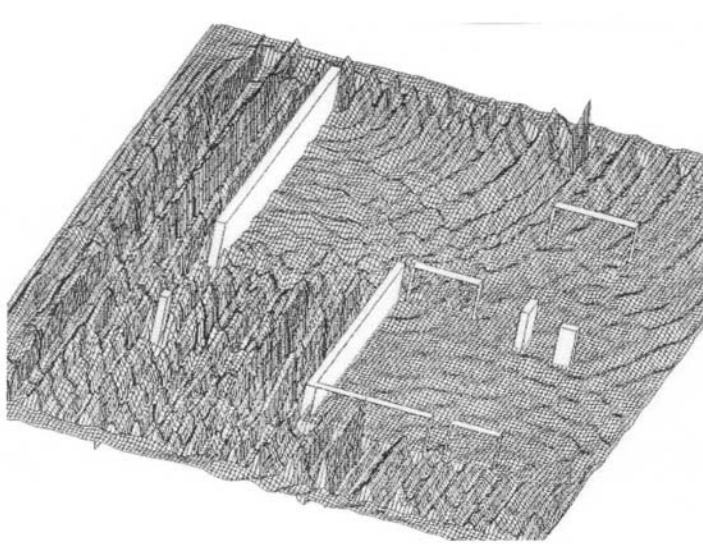

Fig.17 Simulated wave field around breakwater segments of a harbor under construction

Fig.18 shows a simulated image of the wave penetration in the vicinity of the wharf of a deep fishery harbor. In this application, the integrated system was used to determine the effects of a proposed vertical-wall caisson breakwater in front of the wharf on the wave climate inside the harbor and on the tranquility of the wave field in the offshore region. An important result needed from the study is the spatial distribution of the significant wave period, which is used by fishermen to assess the suitability of unloading their catch in the docks. Another important result is the directional distribution of wave energy outside the harbor, which is significantly modified by the scattering of the reflected waves from the breakwater. This information is needed in studying the level of agitation at the entranceways that can be expected by maritime vessels that take refuge or dock

inside the harbor. Images such as these provide a rapid assessment of the locations of wave energy concentration due to multi-reflection within the harbor.
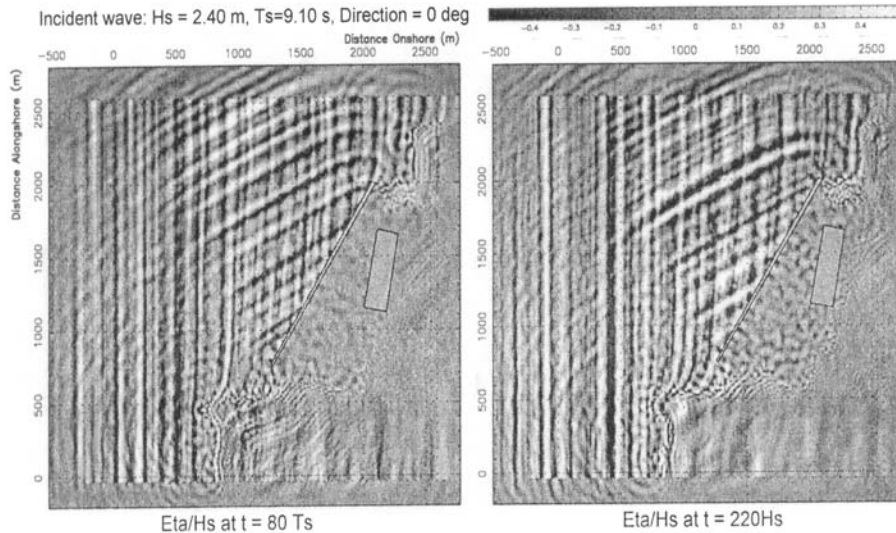

Fig.18 Wave penetration in a deep fishery harbor

VIII. Concluding Remarks

An integrated system of numerical simulation and graphic visualization of wave penetration in harbors has been developed for use in personal computers. The computation engine is based on a mathematical model of nonlinear dispersive waves on arbitrary bottom topography, and incorporates the effects of wave breaking, energy damping around structures, bottom friction, partially reflective boundaries, and open boundaries. The numerical implementation is based on the finite difference method with an alternating-direction-implicit (ADI) scheme on staggered grids. The visualization component is a graphical rendering suite of higher-level routines developed from a set of primitives and low-level graphic routines from an open-source graphics library. Visualization may be performed for pre-processing input and diagnostic data, rendering transient output, and post-processing time series output and other data from the simulation.

The accuracy of the system was verified by comparing its simulated results with the analytical solution for diffraction by a semi-infinite breakwater, with physical model measurements for a rectangular island, and with field measurements of significant waves in a prototype harbor. The simulated results closely agree with theory and physical model data under the same idealized conditions. The simulated wave properties also agree with the field data within

reasonable limits, notwithstanding the differences between the field and simulation conditions.

The integrated system has been applied to study wave penetration in actual harbors. The system provides quick and meaningful images of the wave fields and can be used for purposes of technical analysis, engineering design, scientific study, and construction monitoring and planning.

As a concluding note, an integrated system similar to the present system is currently installed in a network of remote computers. Such network provides field engineers with a quick way of analyzing and visualizing the wave field under actual site conditions for construction planning and field monitoring purposes (Ishikura et al, 1997).

IX.   Acknowledgment

References

1. Berkhoff, J.C.W. "Computation of combined refraction-diffraction". *Proceedings, 13th International Conference on Coastal Engineering.* Vol.1, 191-203. (1972).
2. Cruz, E.C. "Modeling of nonlinear dispersive wave transformation around submerged porous breakwaters". *Doctoral dissertation*, Dept. Civil Eng., Univ. of Tokyo. (1994)
3. Cruz, E.C. "Characteristics of long period oscillations in a harbor based on field measurements". *Proceedings, 5th International Symposium in Civil Engineering.* (in CD-Rom) (2002).
4. Cruz, E.C. "Development of a PC-based visualization suite from an open-source graphic library". *(manuscript in preparation).* (2003).
5. Cruz, E.C. and Isobe, M. "Numerical wave absorbers for short and long wave modeling". *Proceedings, International Symposium on Waves – Physical and Numerical Modeling.* Vol.2, 992-1001. (1994).
6. Cruz, E.C. and Aono, T. "Simulation of nonlinear wave field induced by partially reflective harbors". *Proceedings, Joint 13th Australasian Coastal and Ocean Engineering Conference and 16th Australian Port and Harbor Conference*, Vol.1, 947-952. (1997a).
7. Cruz, E.C. and Aono T. "Investigation of long period oscillations in an enclosed harbor". *Philippine Engineering Journal*, Vol.18, No.2, 15-58. (1997b).

8. Cruz, E.C. and Aono, T. "Wave and current fields around gapped submerged breakwaters". *Journal of Hydraulics, Coastal and Environmental Engineering.* JSCE. Vol.II-42. No.586, pp.127-135. (1998).

9. Cruz, E.C., Isobe, M. and Watanabe, A. "Business Equations for Wave Transformation on Porous Beds". *Coastal Engineering.* Vol. 30. Nos. 1-2. pp. 125-156. (1997).

10. Dean, R. and Dalrymple, R. "Water Wave Mechanics for Engineers and Scientists". Singapore: World Scientific. (1992).

11. http://www.astro.caltech.edu/~tjp/pgplot/

12. Ishii, T., Isobe, M. and Watanabe, A.   " Improved boundary conditions to a time-dependent mild-slope equation for random waves". *Proceedings, 24th International Conference on Coastal Engineering.* Vol.1, 272-284. (1994).

13. Ishikura, M., Cruz, E.C. and Aono, T. "Development of a remote numerical analysis system using Java and VRML". *Proceedings, 22nd Symposium on Civil Engineering Information Processing Systems.* JSCE. Vol.6, 187-190 (in Japanese). (1997).

14. Isobe, M. "Time-dependent mild-slope equations for random waves". *Proceedings, 24th International Conference on Coastal Engineering.* Vol.1, 285-299. (1994).

15. Madsen, P.A. and Sorensen, O.R.   "A new form of Boussinesq equations with improved linear dispersion characteristics". *Coastal Engineering*, Vol.15, 371-388. (1991).

16. Nadaoka, K., Beji, S. and Nakagawa, Y. "A fully dispersive nonlinear wave model and its numerical solutions". *Proceedings, 24th International Conference on Coastal Engineering.*Vol.1, 427-441. (1994).

17. Penney, W.G., and Price, A.T. "The diffraction theory of sea waves and the shelter afforded by breakwaters". *Philosophical Transactions Royal Society* A, Vol. 244(882), 236-253. (1952).

18. Peregrine, D.H "Long waves on beaches". *Journal of Fluid Mechanics.* Vol.27(4), 815-827. (1967).

19. Sato, N., Isobe, M. and Izumiya, T. "A numerical model for calculating wave height distribution in a harbor of arbitrary shape". *Coastal Engineering in Japan*, Vol.33, No.2, 119-131. (1990).